

MAGNETISM IN HIGHLY ANISOTROPIC BORATES: EXPERIMENT AND THEORY

M.A. Continentino, J.C. Fernandes, R.B. Guimarães, B. Boechat and A. Saguia
Instituto de Física, Universidade Federal Fluminense,
Av. Litorânea, s/n, Campus da Praia Vermelha
Niterói, 24.210-340, RJ, Brazil.

1.INTRODUCTION

Highly anisotropic organic and inorganic materials have been the object of intensive studies in the last decades. High T_c superconductivity, quantum Hall effect, charge and spin density waves, disordered magnetic chains, plateau magnetization, solitons and many other phenomena are examples of the physical richness presented by this large class of compounds. It is not surprising that anisotropic materials became so attractive for solid state physicists.

The $3d$ metal anhydrous borates, in which the boron ions have trigonal coordination forming the orthoborate $(BO_3)^{3-}$ or pyroborate $(B_2O_5)^{4-}$ anion groups, present high internal anisotropy revealed by the morphology of their crystals which appear as needles or plaquettes. The anhydrous borates possessing the orthoborate group are called orthoborates and frequently oxy-borates since, in these compounds, there are one or two oxygen ions per chemical formula not directly bound to the boron ions. The oxy-borates present more than ten different crystallographic structures among which the warwickites and ludwigites are the easiest to be synthesized. The borates possessing the pyroborate

groups are simply called pyroborates. They form a smaller class of compounds, also easy to be synthesized, but having all the oxygen ions within the borate groups. The borates for which the boron ions have tetrahedral coordination do not present any remarkable anisotropy. We may claim therefore that the high anisotropy in the anhydrous borates is a consequence of the boron trigonal coordination. It must be remarked that, since the borate anions in the anhydrous borates are isolated, they do not form polymerized subsystems as chains or planes. Chains or planes of anions groups appear in other borates as well as in many silicates in which the $(SiO_4)^{4-}$ or $(Si_2O_7)^{6-}$ tetrahedra form low-dimensional subsystems [1]. The number of oxy-borates with different crystallographic structure and chemical composition is very large so that the study of their physical properties is far from being exhausted. We may mention, as an example, the physical properties of bi-dimensional oxy-borates which have never been investigated. In this chapter we present an overview of the main magnetic properties of warwickites and ludwigites as well as those of two pyroborates. For the detailed properties of these compounds the reader will be referred to the original papers. Only the borates whose magnetic properties were investigated are addressed. The theoretical aspects of some specific phenomena presented by these borates will be discussed.

2. THE ANHYDROUS BORATES

There are three main groups of anhydrous borates: the warwickite group, the ludwigite or pinakiolite group and the pyroborate group. The respective general chemical formulae are: $M^{3+}M'^{2+}OBO_3$, $M^{3+}(M'^{2+})_2O_2BO_3$ and $M^{2+}M'^{2+}B_2O_5$ where M and M' represent different metals. If $M = M'$ the borate is said to be *homo-metallic*, otherwise it is *hetero-metallic*. There are also smaller groups of orthoborates and mixed ortho-pyroborates which will not be considered here. In any anhydrous borate the metals M and M' are found within an oxygen octahedra and every metal site of each structure may be randomly occupied by M or M' with different probabilities. For this reason hetero-metallic anhydrous borates are always disordered.

2.1 The Warwickites

Table 1 presents the symmetry space groups for the warwickites. All the hetero-metallic warwickites belong to the same space group [6]. The schematic structure of the warwickites projected on the plane ab is shown in Fig. 1. We can observe, in this figure, parallelograms which are orthogonal sections of substructures, similar to ribbons, indefinitely extended along the c axis. Such ribbons are formed by oxygen octahedra packed in the hexagonal form and sharing edges in such a way that three of their vertices lie on each one of the larger faces of the ribbons. These octahedra give rise to four columns, along the ribbons, and their centers define two types of equivalent crystallographic sites: those on the border (sites 2) and those on the middle of the ribbons (sites 1). These sites

form a triangular lattice and are randomly occupied by M or M' as shown in Fig. 2.

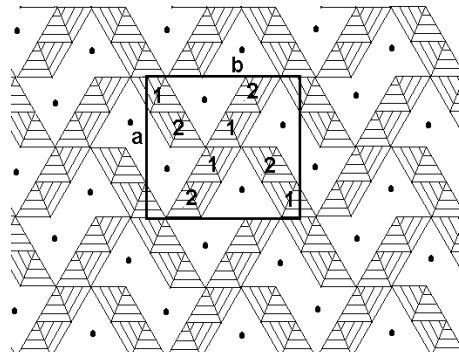


Figure 1: The structure of the warwickites projected in the plane ab . The sides a and b of the unitary cell and the crystallographic sites 1 and 2 are shown. The full circles represent the boron ions [6].

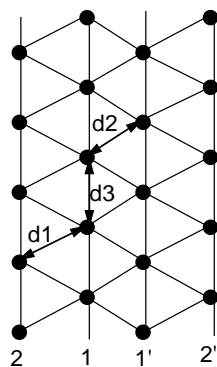


Figure 2: The internal structure of one ribbon. The full circles represent the metal ions. The numbers stand for the crystallographic site correspondent to each column and the d 's are the intermetallic distances [7].

2.2 The Ludwigites

The ludwigite or pinakiolite group includes several crystalline structures under the general chemical formula given above. The more complex structures are stabilized by impurities. Table 2 gives the space group and one correspondent typical chemical composition for each structure belonging to this group. The schematic structure of the ludwigites $Pbam$ projected on the plane ab is shown in Fig. 3. The zig-zag walls, called F walls by Norrestam and Bovin [15], have an hexagonal internal structure. However, the shortest distances between metals are found within the three column wall, also called C wall, formed by

Compound	<i>space group</i>	<i>ref.</i>
$MgScOBO_3$	$Pnam$	[2]
Mn_2OBO_3	$P2_1/n$	[3]
Fe_2OBO_3	$Pm\bar{c}n$ above 317K	[4, 5]
Fe_2OBO_3	$P2_1/c$ below 317K	[4, 5]

Table 1: Space group of symmetry for the synthetic warwickites. The hetero-metallic warwickites have all the same space group.

columns of the crystallographic sites 4-2-4. Within these walls the metal sites form a three leg ladder rectangular lattice (see Fig. 4).

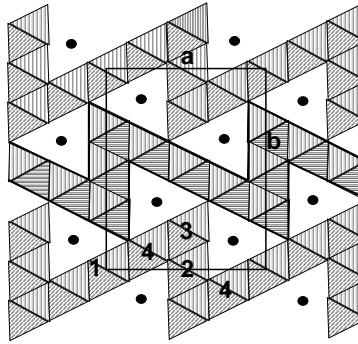


Figure 3: The structure of the ludwigites $Pbam$ projected on the ab plane. The sides a and b of the unit cell and the numbers of the metal sites are shown. The full circles represent the boron ions [8].

2.3 The Pyroborates

The two pyroborates whose magnetic properties have been studied are the homo-metallic $Mn_2B_2O_5$ [17] and the hetero-metallic $MnMgB_2O_5$ [17, 18, 19]. Both are electrically insulating. In Fig. 5 it is shown the schematic structure of the pyroborates projected in the plane bc . In this figure, the ribbons and the anion groups $(B_2O_5)^{4-}$ appear clearly. It is to be remarked that the ribbons do not "touch" as in the warwickites.

3. MAGNETIC PROPERTIES

Wiedenmann et al. [20, 21] have probably been the first authors to point out the existence of quasi one-dimensional interactions in oxy-borates when studying the magnetic properties of $MgFeOBO_3$ and $Mg_2FeO_2BO_3$. However, the experimental and theoretic-

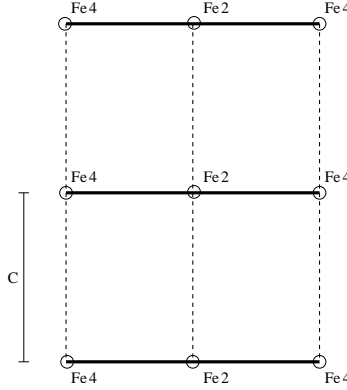


Figure 4: The internal structure of one C wall formed by three columns correspondent to sites 4-2-4. Such structure is called a three leg ladder [16].

name	chemical formula	s.g.	ref.
<i>ludwigite</i> (*)	$Co_3O_2BO_3$	<i>Pbam</i>	[8]
<i>ludwigite</i> (*)	$Cu_2FeO_2BO_3$	<i>P2₁/c</i>	[9]
<i>hulsite</i>	$Mg_{0.64}(Fe^{2+})_{1.46}(Fe^{3+})_{.67}(Sn^{4+})_{.20}O_2BO_3$	<i>P2/m</i>	[10]
<i>Pinakiolite</i>	$Mg_{1.68}(Mn^{2+})_{.09}Mn^{3+}(Al, Fe, Mn)_{.11}BO_5$	<i>C2/m</i>	[11]
<i>Orthopinakiolite</i>	$Mg_{1.42}(Mn^{2+})_{.43}(Mn^{3+})_{.88}(Fe^{3+})_{.22}BO_5$	<i>Pnmm</i>	[12]
<i>Takeuchiite</i>	$Mg_{1.59}(Mn^{2+})_{.42}(Mn^{3+})_{.78}(Fe^{3+})_{.19}(Ti^{4+})_{.01}BO_5$	<i>Pnmm</i>	[13]
<i>Blatterite</i>	$Mg_{1.33}Mn_{1.44}Fe_{.05}Sb_{.17}O_2BO_3$	<i>Pnmm</i>	[14]

Table 2: Space group of symmetry and chemical composition for synthetic (*) and mineral compounds with general chemical formula $M^{3+}(M'^{2+})_2O_2BO_3$.

cally supported existence of random magnetic chains in oxy-borates was firstly shown by Fernandes et al. in the warwickite $MgTiOBO_3$ [22]. These authors verified that the temperature dependences of the susceptibility and magnetization in this oxy-borate are the same as those in the one-dimensional organic compounds based on the *TCNQ* molecule, as reported by Boulaevskii et al. [23]. In this way the warwickite $MgTiOBO_3$ was the first inorganic compound found to present random quantum magnetic chain type of behavior. Its electronic structure has been theoretically investigated by Matos et al. [24] and by Marcucci et al. [25] and its low dimensionality has been confirmed. All the studied hetero-metallic borates, with boron in trigonal coordination, present similar magnetic behavior.

The homo-metallic borates have not an uniform behavior. The pyroborate $Mn_2B_2O_5$ exhibits the more interesting consequence of quasi one-dimensional magnetic interactions: its magnetization curve presents several inflection points indicating a hierarchy of such interactions [17]. In turn, the only known homo-metallic warwickites, Mn_2OBO_3 and Fe_2OBO_3 , do not present any evidence of low dimensional magnetic interactions [26]. Charge ordering and magnetism seems to be dissociated in the homo-metallic borates ex-

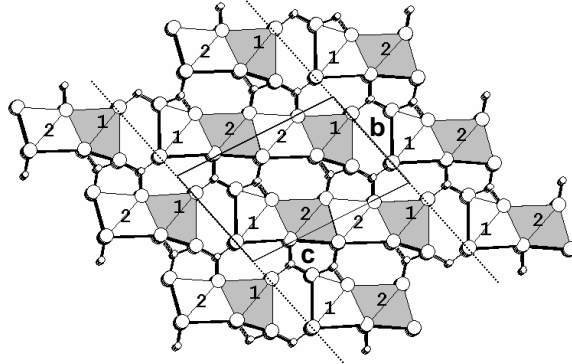


Figure 5: The structure of the pyroborate projected in the plane bc . We notice the ribbons, the borate groups and the sides b and c of the unit cell. The largest circles indicate oxygen ions while the smallest ones indicate the boron ions [18].

ception, perhaps, in the iron ludwigite $Fe_3O_2BO_3$ whose magnetic susceptibility presents an anomaly in the temperature region where a structural phase transition occurs [16]. As will be seen below, the low temperature phase associated to this transition presents charge density waves or, what is the same, structural anisotropy and long range charge ordering.

3.1 Hetero-metallic Borates

The hetero-metallic borates are naturally disordered materials since each metal crystalline site may be occupied by any one of the two metals which appear in the chemical formula. Both these metals may be magnetic ($3d$ metals) but in the majority of the studied hetero-metallic borates only one metal is magnetic. This disorder generates a spectrum of intensities for the exchange and super-exchange interactions between the magnetic ions. In highly anisotropic borates such spectrum yields to disordered quantum magnetic chain type of behavior. The magnetic properties of the hetero-metallic borates show clearly the characteristic power law behavior associated with these random chains whatever is the respective crystalline structure: warwickite, ludwigite or pyroborate. The magnetic susceptibilities of the hetero-metallic warwickites and pyroborates depend very similarly on the temperature. For sufficiently high temperatures these materials are paramagnetic and obey the Curie-Weiss law with antiferromagnetic exchange interaction between nearest neighbors. As temperature is lowered, a short range interaction appears within the ribbon since $k_B T$ approaches the intra-ribbon exchange energy between magnetic ions.

In this temperature range the susceptibility is larger than that given by the Curie-Weiss law and depends on the temperature as a power law. This is the temperature range for which the magnetic behavior of the system is that of a random magnetic chain. Further decreasing temperature there is eventually a spin glass transition at T_{sg} when the interaction between ions in adjacent chains becomes larger than $k_B T$. This transition is essentially a tri-dimensional (3D) phenomenon involving the whole system. This is the case in hetero-metallic warwickites and pyroborates. The spin glass nature of the transition is evident from the frequency dependence of the cusp in the a.c. susceptibility curve at T_{sg} . Fig. 6 and Fig. 7 show the magnetic susceptibility of $MgTiOBO_3$ [22] and $MgVOBO_3$ [27] respectively. The cusp at 6 K in the $MgVOBO_3$ curve indicates a spin-glass freezing. For $MgTiOBO_3$ no transition has been found down to 300 mK [28].

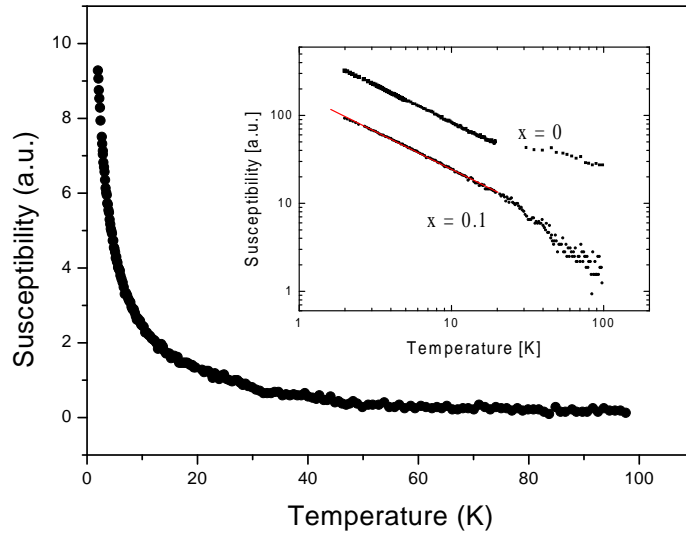


Figure 6: a.c. susceptibilities of the $Mg_{1-x}Ti_{1+x}OBO_3$ warwickites as a function of temperature for $x=0$ and $x=0.1$. The inset shows the power law behavior [22].

Bulaevskii et al. [23] developed a theory to account for the magnetic susceptibility χ and specific heat C temperature dependences of spin-1/2 random magnetic chains present in compounds based on the *TCNQ* molecules. They also found an expression for the applied field dependence of the magnetization m in the field region where $k_B T \ll g\mu_B H \ll J$. In this inequality J is the highest exchange interaction in the chain. According to these authors:

$$\chi \propto T^{-\alpha} \quad (1)$$

$$C \propto T^{1-\alpha} \quad (2)$$

and

$$m \propto H^{1-\alpha} \quad (3)$$

where α is a weakly temperature dependent parameter. The above equations characterize the thermodynamic behavior of random spin-1/2 magnetic chains. Later on in this

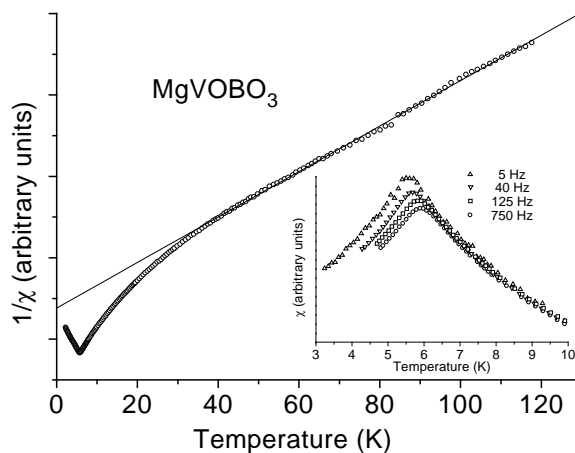


Figure 7: a.c. susceptibility of powdered $MgVOBO_3$ as a function of temperature for a frequency of 125 Hz and an alternating field of 10 Oe. The cusp at $T_{sg} = 6$ K is associated with a spin-glass transition. The inset on a logarithmic scale shows the power-law behavior of the susceptibility for $T > T_{sg}$ [27].

chapter we shall discuss in detail the physical nature of the power law dependence of these thermodynamic quantities and the case of random magnetic chains with spins larger than $1/2$. In Table 3 are listed the studied hetero-metallic warwickites and pyroborates with respective relevant magnetic parameters.

In the iron ludwigites, if the divalent metal is magnetic, each metallic subsystem orders at different temperatures allowing the coexistence of magnetic order and paramagnetism. This is the case of $Ni_2FeO_2BO_3$ [29] and $Cu_2FeO_2BO_3$ [30]. The homo-metallic ludwigite $Fe_3O_2BO_3$ also present two different critical temperatures. This may be clearly seen in the Mössbauer spectra shown in Fig. 8 [31]. This compound will be discussed in detail below. In Table 4 are listed the iron ludwigites with the ordering temperatures of the iron

Compound	$T_{sg}(K)$	α	ref.
$MgTiOBO_3$	< 0.3	0.83	[22, 28]
$MgVOBO_3$	6	0.54	[27]
$MgCrOBO_3$	6.5	0.66	[7]
$MgFeOBO_3$	11	0.54	[7]
$ScNiOBO_3$	6	0.55	[7]
$ScMnOBO_3$	2.7	0.50	[7]
$MnMgB_2O_5$	0.6	0.56	[19]

Table 3: Spin glass temperature, and the alpha parameter for hetero-metallic warwickites and pyroborates.

Compound	$T_{iron}(K)$	$T_{div}(K)$	<i>ref.</i>
$Mg_2FeO_2BO_3$	10	--	[32]
$Fe_2FeO_2BO_3$	112	70	[31]
$Ni_2FeO_2BO_3$	106	46	[29]
$Cu_2FeO_2BO_3$	60	40	[30]

Table 4: Ordering temperatures for the metallic subsystems in iron ludwigites. T_{iron} stands for the iron subsystem and T_{div} . for the divalent metal subsystem

and of the divalent metal subsystems. These are T_{iron} and T_{div} , respectively.

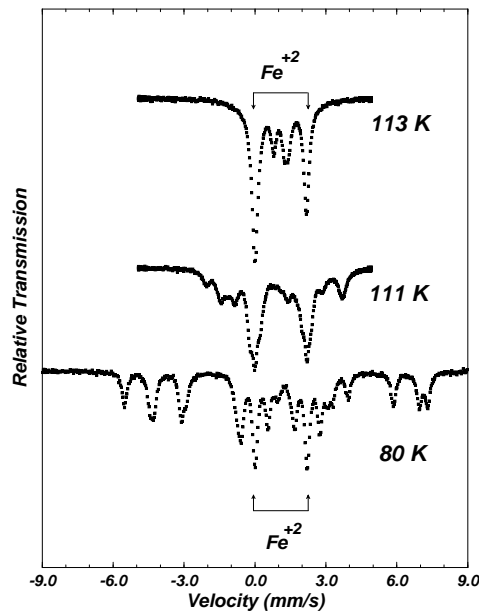


Figure 8: Mössbauer spectra of $Fe_3O_2BO_3$ at selected temperatures above and below T_{iron} [31].

The hetero-metallic pyroborate $MnMgB_2O_5$ behaves essentially as an hetero-metallic warwickite. Its T_{sg} is however much lower (≈ 600 mK) [19] since, in this compound, the ribbons do not touch.

3.2 Homo-metallic Borates

The homo-metallic borates, with different ions of the same metal, present electrical conductivity and long-range charge ordering which is associated, in general, with a structural transition. In this case the metal is necessarily a $3d$ metal so that such borates are magnetic. In the case of identical ions, as in the pyroborate $Mn_2B_2O_5$, the material

Compound	$T_{struc}(K)$	$T_{mag}(K)$	T'_{mag}	<i>ref.</i>
$Mn_2B_2O_5$	— — —	23.3	—	[17]
Fe_2OBO_3	317	155	—	[5, 33]
Mn_2OBO_3	> 300	104, 26	—	[26, 34]
$Fe_3O_2BO_3$	283	112	70	[16, 31]

Table 5: Structural transition and magnetic ordering temperatures for the homo-metallic borates.

is electrically insulating and does not present any structural transition. The compound $Mn_2B_2O_5$ is an ordinary antiferromagnet with no net magnetization below its ordering temperature since there is no ESR signal in the ordered phase [17]. It presents a magnetization curve, measured in single crystals, showing some inflection points which indicate the intra-ribbons and inter-ribbons exchange values. Its magnetic ordering configuration is not yet known. The two known homo-metallic warwickites have magnetic critical temperatures much larger than the hetero-metallic spin glass critical temperatures. Their magnetic order configurations are not very simple: *L*-type ferrimagnetism in Fe_2OBO_3 [5, 33] and a complex ordering pattern in Mn_2OBO_3 presenting considerable frustration [34]. The last studied homo-metallic borate is the iron ludwigite $Fe_3O_2BO_3$. Its magnetic behavior is very intricate [31, 35] and its specific heat is rigorously linear between 70 K and 200 K [36]. Its internal anisotropy becomes evident through its needle shaped single crystals. There is a structural transition at 283 K and the low temperature phase presents charge density waves along the crystal *c* axis which is the needles axis. It must be remarked that the crystals of the pyroborate $Mn_2B_2O_5$ and of the ludwigite $Fe_3O_2BO_3$ are clearly needle shaped attaining easily more than 2 mm in length. For the homo-metallic warwickites their crystals are so small that it is impossible to determine clearly their morphology with the only aid of an optical microscope. This is compatible with the absence of low-dimensional features in their properties. Table 5 shows some magnetic parameters of the homo-metallic borates.

4.CHARGE ORDERING AND STRUCTURAL TRANSITION

As pointed out before, the homo-metallic oxy-borates have two different ions of the same metal. An ordered configuration of such ions, simultaneous to a structural phase transition, appears in these compounds as the temperature is lowered below a characteristic temperature T_c . The ordered charge configuration is different in each compound so that different mechanisms were considered responsible for the respective ordering processes.

The structure of the warwickite Mn_2OBO_3 can be considered to be a distorted modification of the orthorhombic warwickite structure. Following Norrestam et al. [3], the distortions, apparently caused by Jahn-Teller effects induced by the Mn^{3+} ions, remove the mirror symmetry of the parent undistorted warwickite. As a consequence, its space group is the monoclinic $P2_1/n$. The bond distances and calculated bond valence sums

indicate that, in the charge ordered state, the trivalent manganese ions are located in the two inner columns of the ribbons so that the divalent ones are in the two outer columns [3]. The probable T_c is not known for this compound since X-ray diffraction measurements have not been performed above room temperature.

Attfield et al. [4, 5] observed that the homo-metallic warwickite Fe_2OBO_3 presents a charge ordered phase below $T_c = 317$ K in which the divalent and trivalent iron ions are equally distributed over the structurally distinct iron sites 1 and 2 shown in Fig. 1. Above T_c the structure is orthorhombic with space group $Pm\bar{c}n$ and below this temperature the space group is the monoclinic $P2_1/c$. These authors suggest that, in this case, the ordering mechanism is the electrostatic repulsion.

The homo-metallic ludwigite $Fe_3O_2BO_3$, as the warwickites, also presents a structural phase transition. In this case $T_c = 283$ K [16]. The high temperature space group is the orthorhombic $Pbam$ (n° 55) and below T_c the space group is the orthorhombic $Pbnm$ (n° 62). As the temperature goes below T_c , the only important change in the structure appears within the three leg ladders in the C walls (see section 2.2). The columns of sites 2 are zig-zag distorted, as seen in Fig. 9, so that the c edge of the unit cell is doubled relatively to the high temperature phase. Mössbauer Spectroscopy indicates that, below room temperature, the ions Fe^{2+} in sites 2 share electrons with ions Fe^{3+} in sites 4 so that $Fe^{2.5+}$ ions appear [37, 38]. Latgé and Continentino [39] proposed that this sharing is performed between site 2 and the nearest site 4a so that a transverse charge density wave arises along the c axis. These authors have shown that, if the ladder is viewed as a background of localized Fe^{3+} ions where the extra electrons of the Fe^{2+} ions are itinerant in a tight-binding band with infinite local repulsion, the distortion of the ladder lowers the total electronic energy. The magnetic character of the ions involved in the charge density wave has led Whangbo et al. [40] to suggest a magnetic mechanism as the cause of the structural instability of $Fe_3O_2BO_3$.

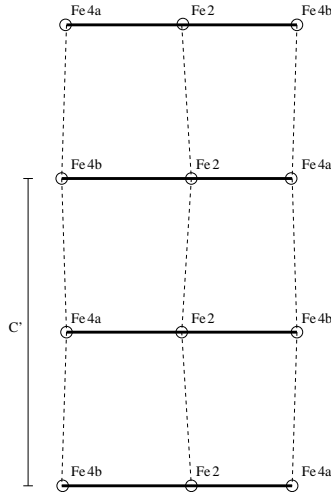


Figure 9: The three leg ladder which constitutes the C wall at $T < T_c$ [16].

5.RANDOM MAGNETIC CHAINS

The results on the magnetic properties of the oxy-borates presented in the previous sections provide a strong motivation to investigate theoretically these materials. The actual low dimensional structures which are relevant for the understanding of the magnetic behavior of the oxy-borates are ladders. In the case of the warwickites, four leg ladders in the ribbons (see Fig. 2) and for the ludwigites, three leg ladders (see Fig. 4). The Hamiltonian we will consider is the Heisenberg model describing local moments with spin $-S$ on the sites of a ladder interacting mostly through super-exchange interactions. This is appropriate since the $d - d$ overlap is not very significant in these materials although alternative approaches have been proposed [25, 40]. For the purpose of describing the magnetic properties of the oxy-borates, a localized Heisenberg model is adequate. Since in the hetero-metallic materials the occupation of these sites is random, this gives rise to a distribution of magnetic couplings. The properties of random Heisenberg ladders have been the subject of intense studies in the last years [41, 42, 43]. Mostly of these investigations have concentrated in the case of the spin $-1/2$, two leg ladder (2LL) and the spin $-1/2$ zig-zag ladder (ZZL) [42, 43]. The latter is topologically equivalent to single chains with nearest and next-nearest neighbors interactions. However, both ladders map into a random single chain problem, either with half-integer or integer spins. Additionally, the 2LL and zig-zag ladders lead to effective low energy models with only nearest neighbor interactions [42]. We may expect these results to hold for ladders with an arbitrarily finite number of legs for sufficiently low temperatures or energy scales. Consequently, the study of quantum random chains is essential for understanding the magnetic properties of low dimensional oxy-borates. Notice that for the pure case with no disorder, spin $-1/2$ ladders with an even number of legs map into the spin -1 chain problem while those with an odd number of legs map into the spin $-1/2$ case [41].

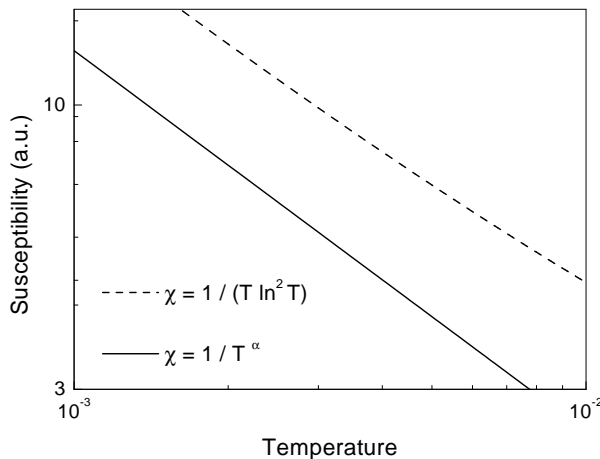


Figure 10: Susceptibility as a function of temperature comparing the power law behavior with a temperature independent exponent ($\alpha = 0.7$) and the random singlet phase result.

The nature of the low energy phases found in random Heisenberg chains and conse-

quently in ladders are mainly of four types,

- A random singlet phase which is typical of random Heisenberg antiferromagnetic spin-1/2 chains. This phase is associated with an infinite randomness fixed point and low temperature thermodynamic properties characterized by power law behavior with exponents which depend weakly on temperature. The magnetic susceptibility $\chi(T) \propto T^{-\alpha}$, the specific heat $C/T \propto T^{1-\alpha}$ and the magnetization m as a function of the external magnetic field H varies as, $m(H) \propto H^{1-\alpha}$. These expressions with a temperature dependent exponent $\alpha(T)$ are useful representations of the actual temperature dependence of these quantities in the random singlet phase. For the magnetic susceptibility this is, $\chi \propto 1/(T \ln^2 T)$ and the free energy $F \propto T^2/(\ln^2 T)$.
- A Griffiths phase which is also characterized by power law behavior of the thermodynamic quantities, as in the previous case. It is distinguished from the random singlet phase by the fact that the relevant exponents depend on the distance δ to an infinite randomness quantum critical point, i.e., to the amount of disorder in the system. The susceptibility in the Griffiths phase is given by, $\chi(T) \propto T^{1/Z_\kappa(\delta)-1}$, where Z is the *dynamic exponent*. The specific heat in this phase is given by, $C(T)/T \propto T^{-1+1/Z_\kappa(\delta)}$ and for small magnetic fields H , the magnetization, $m \propto H^{1/Z_\kappa(\delta)}$. The dynamic exponent Z assumes the values $Z = \infty$ at the infinite randomness fixed point, i.e., at the random singlet phase ($\delta = 0$) and $Z = 1$ at the border of the Griffiths phase ($|\delta| = \delta_G$). The dynamic exponent is obtained from the *first gap distributions* [44] that saturate at low energies in the form, $P(-\log \Delta) \sim \Delta^{1/Z}$ for $\Delta \rightarrow 0$.
- A large spin (LS) phase characteristic of random magnetic chains with both ferromagnetic and antiferromagnetic interactions [45]. For weak disorder this phase shows universal behavior with a Curie like divergence of the magnetic susceptibility, $\chi(T) \propto 1/T$ and a specific heat that vanishes as, $C \propto T^{1/Z} |\ln T|$ with a constant dynamic exponent $Z \approx 0.44$. For strong randomness Z starts to vary with disorder but the magnetic susceptibility is still Curie-like. This phase is relevant for the antiferromagnetic zig-zag ladders which for strong and random next nearest neighbors interactions eventually map into a single chain problem with ferro and antiferromagnetic couplings. In the case of the oxy-borates the interactions are antiferromagnetic. There is in these materials, at high temperatures, a linear temperature dependent susceptibility but always with a finite negative paramagnetic Curie temperature, such that, this behavior can not be attributed to a LS phase.
- There is also for weak disorder a random dimer, Haldane-like gapped phase with vanishing susceptibility or still regions of the phase diagram where the dynamic exponent Z is constant [42].

It should also be noticed that experimentally it is not an easy matter to distinguish between the random singlet phase from the Griffiths phase. In Figure 10 we show a schematic plot of the magnetic susceptibility to illustrate this point. On the other hand the

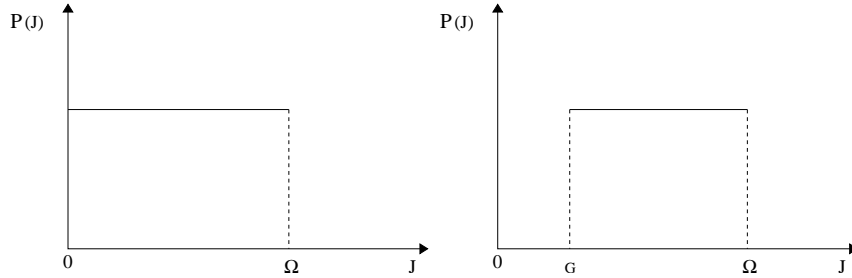


Figure 11: Initial distributions of interactions used in the renormalization group calculations. In the strong disorder case $G = 0$.

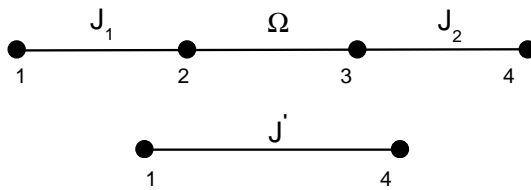


Figure 12: The MDH elimination procedures. Ω is the largest interaction in the chain. The strongest coupled pair of spins, 2 and 3 is eliminated giving rise to an effective interaction J' between spins 1 and 4.

LS phase is clearly characterized by the Curie-like behavior of the magnetic susceptibility. Having established that the low temperature phases of random magnetic ladders are similar in nature to those of random single chains we present below a study of the phase diagrams of the latter.

The random exchange Heisenberg antiferromagnetic chain (REHAC) plays a fundamental and paradigmatic role in the study of disordered quantum systems. Their study was initially motivated by experimental results in disordered organic chain materials which presented peculiar behavior [23]. Essentially, a magnetic susceptibility which diverges, at low temperatures, as a power law of temperature with an exponent $\alpha < 1$. The initial theoretical approaches to this problem associated this behavior with a distribution of exchange couplings with similar power law dependence, $P(J) \propto J^{-\alpha}$. A breakthrough from the theoretical side was the introduction by Ma, Dasgupta and Hu (MDH) [46] of a perturbative renormalization group method to treat the random Heisenberg chain. The REHAC system is defined by the following Hamiltonian for a chain of L spins:

$$H = \sum_{i=1}^{L-1} J_i \vec{S}_i \cdot \vec{S}_{i+1}, \quad (4)$$

where \vec{S}_i are spin-1/2 operators and J_i are positive random nearest neighbor interactions, taken from a distribution $P(J_i)$ with a cut-off Ω (see Fig. 11).

The MDH method consists in identifying the pair of spins with the strongest coupling in the random chain and eliminating it by considering the interaction with the neighboring spins of this pair as a perturbation. This procedure generates new couplings J' between

the two spins neighboring the eliminated pair, as shown in Fig. 12, and consequently the form of the distribution $P(J)$ is modified. One also gains a contribution to the free energy of the system from the eliminated pair. This process is then successively applied until a single pair of spins remains. The new effective coupling is given by,

$$J' = \frac{1}{2} \frac{J_1 J_2}{\Omega}. \quad (5)$$

Along the RG procedure, *independent of the initial distribution* $P(J)$, the system flows to an *infinite randomness fixed point* characterized by the fixed point form of the probability distribution of interactions given by

$$P(J) = \frac{\alpha}{\Omega} \left(\frac{\Omega}{J} \right)^{1-\alpha} \quad (6)$$

At zero temperature, the exponent α is a function of the cut-off Ω of the distribution and varies as,

$$\alpha = \frac{-1}{\ln \Omega} \quad (7)$$

This behavior characterizes the so-called random singlet phase [47]. The number of remaining active spins N_R as a function of the energy scale set by the cut-off Ω introduces a new exponent ψ which is defined by,

$$L = \frac{N}{N_R} = \frac{1}{n_\Gamma} = \frac{1}{|\ln \Omega|^{1/\psi}} \quad (8)$$

where N is the number of spins in the original chain. This establishes the connection between the characteristic length L and the energy scale Ω . This is an extension of the usual definition of a dynamic exponent ($\Omega \propto \tau^{-1} \propto L^z$) for the case of logarithmic scaling. For the random singlet phase the exponent ψ takes the value, $\psi = 1/2$. These results are well established for the spin-1/2 REHAC. The convergence of the MDH perturbative procedure for the exact result is guaranteed by the fact that in Eq. 5 the pre-factor (1/2) assures that the new effective interaction J' is always smaller than those eliminated.

In order to generalize the MDH method to spin-1 chains, we consider the general bilinear, biquadratic, spin-1 chain [48] with L spins described by the Hamiltonian

$$H = \sum_{r=1}^{L-1} J_r \vec{S}_r \cdot \vec{S}_{r+1} - \sum_{r=1}^{L-1} D_r (\vec{S}_r \cdot \vec{S}_{r+1})^2 \quad (9)$$

where J_r and D_r are random nearest-neighbor interactions with probability distributions $P_J(J_r)$ and $P_D(D_r)$ respectively and such that $0 \leq J_r \leq J$ and $0 \leq D_r \leq D$. The \vec{S}_r are spin-1 operators and we are interested in the limit $L \rightarrow \infty$.

For the case of purely biquadratic interactions and no exchange we assume a distribution of random biquadratic couplings and take $J_r = 0$. Generalizing the procedure of Ma et al. [46] for this problem, we identify the pair of spins with the strongest biquadratic coupling. When we apply the elimination transformation to this strong coupled pair we

find an effective coupling between the spins neighboring the eliminated pair which is given by [48] :

$$D' = \frac{2 D_1 D_2}{9 D} \quad (10)$$

where D_1 and D_2 are the bonds connecting the strongest coupled pair of spins, with interaction strength D , to their neighbors. It is clear that in this case the successive application of the elimination transformation generates weaker and weaker couplings and the distribution of biquadratic interactions becomes peaked close to the origin as the cutoff D decreases. The physical properties of the system are then dominated by low energy excitations and this new phase is very similar to the *random singlet phase* of the disordered spin-1/2 random antiferromagnetic chain [47]. Disorder has a dramatic effect in this case since in the pure case the system has a dimerized phase with a gap for excitations and a short correlation length. The introduction of weak randomness on the biquadratic couplings gives rise to a new disordered phase with low energy excitations and long-range magnetic correlations. This behavior is universal in the sense that, independently of the initial distribution of couplings $P_D(D_r)$, the final distribution converges to a fixed point form which is approximately described by a power law with a singularity at the origin [46]. Notice that the equation above renormalizes to weak coupling faster than that for the spin-1/2 REHAC where the pre-factor of the recursion relation equivalent to Eq. 10 is 1/2 [46]. We have found here a rather unusual situation where a phase with a gap and a short correlation length has become completely unstable and furthermore with long-range magnetic correlations due to the introduction of arbitrarily weak disorder [49].

We include now a weak random exchange interaction between nearest neighbor spins such that the cutoff $J \ll D$. A generalization of the elimination transformation gives, for the new exchange and biquadratic couplings between the spins neighboring the eliminated pair, the following coupled relations [48]

$$D' = \frac{2 D_1 D_2}{9 D + J} \quad (11)$$

$$J' = \frac{4 J_1 J_2}{3 (3D + J)}$$

where as before D_1 , D_2 , J_1 and J_2 are the bonds connecting the strongly coupled pair of spins, with interactions D and J between them, to their neighbors. Since $D \gg J$ we expect, as before, that the renormalized distributions converge rapidly to a weak coupling situation, i.e., to develop more and more weight close to the origin as the cutoff decreases. Again the system attains a random singlet phase dominated by low energy excitations.

In the situation where $D_r = 0$, i.e., for the random exchange spin-1 chain, the elimination procedure yields the following relation for the new coupling between the spins neighboring the eliminated pair [48],

$$J' = \frac{4 J_1 J_2}{3 J} \quad (12)$$

We find here a situation quite different from the previous case, since this recursion relation appears to iterate to strong coupling due to the factor $(4/3) > 1$. The generation of

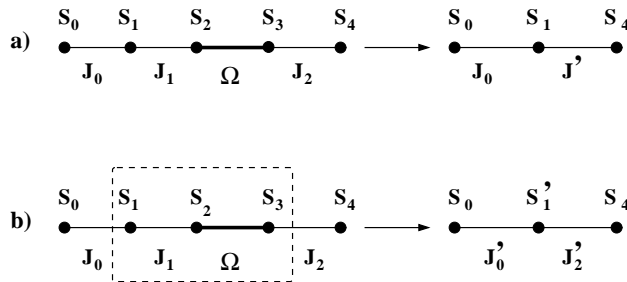


Figure 13: The two elimination procedures as described in the text ($J_1 > J_2$).

couplings which are larger than those eliminated would in fact invalidate the present approach based on perturbation theory. This problem is common to all spins larger than $1/2$. The MDH elimination transformation has been extended for a quantum Heisenberg chain with arbitrary spin S and the following recursion relation has been obtained [48],

$$J' = \frac{2}{3}S(S+1)\frac{J_1J_2}{J} \quad (13)$$

This result shows that perturbation theory in general fails for $S > 1/2$, so that, a universal random singlet phase in the Heisenberg chain with random exchange interactions is guaranteed only for spin- $1/2$ [50, 51, 52]. In this case the quantum fluctuations are sufficiently strong and the renormalization group equations yield a flow to a fixed point, universal distribution, singular at the origin. The above result led to an intense activity to overcome this type of difficulty and to obtain results for quantum random chains of arbitrary spin S . We discuss now the results for spin- 1 chains [44, 53, 54].

Our generalization of the MDH method consists in either of the following procedures shown in Fig. 13 [44]. If the largest neighboring interaction to Ω is $J_1 < (3/4)\Omega$ we eliminate the strongest coupled pair, see Fig. 13a, obtaining an effective interaction between the neighbors to this pair which is given by Eq. 12. This effective interaction is always smaller than those eliminated.

Now suppose $J_1 > (3/4)\Omega$ ($J_1 > J_2$). In this case, we consider the *trio* of spins $S = 1$ coupled by the two strongest interactions of the trio, J_1 and Ω and solve it exactly (see Fig. 13b). The ground state of this trio of spins $S = 1$ is a degenerate triplet and it will be substituted by an effective spin- 1 interacting with its neighbors through new renormalized interactions obtained by degenerate perturbation theory. This procedure which implies diagonalizing the 27×27 matrix of the trio is carried out *analytically*. This is important for obtaining results on large chains and to deal with the large numbers of initial configurations that have been used. These procedures guarantee that we always comply with the criterion of validity of perturbation theory and *never* an interaction larger than those eliminated is generated, as shown in Fig. 14, differently from the MDH scheme.

We consider initial rectangular distributions of antiferromagnetic interactions, $P(J) = [1/(1-G)]\Theta(1-J)\Theta(J-G)$. The gap G is a measure of the amount of disorder being inversely related to it (see Fig. 11). The strong disorder case has $G = 0$ and corresponds to the quantum critical point of the phase diagram of Figure 15. At this point $G = 0$

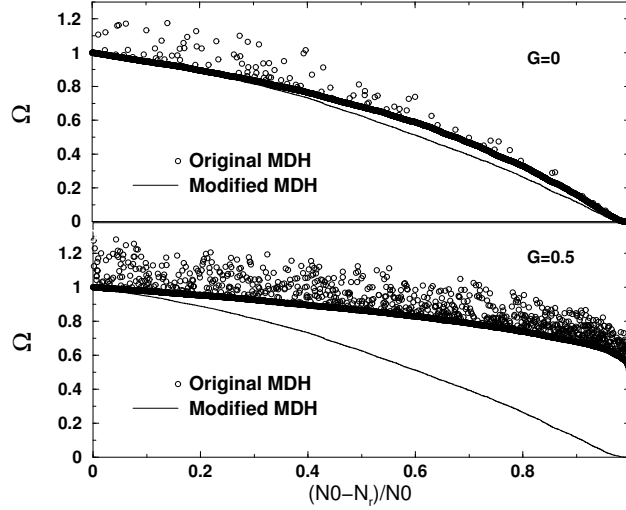


Figure 14: Evolution of the cut-off of the exchange distribution for a random chain as a function of the fraction of eliminated spins for the two renormalization procedures discussed in the text. Note that the naive *MDH* process generates interaction larger than those eliminated, even for strong disorder ($G = 0$). This never occurs in the new procedure used here [44].

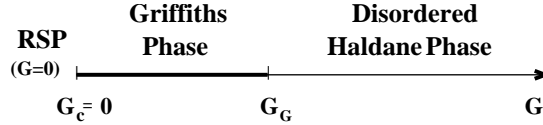


Figure 15: The phase diagram of the spin-1 random Heisenberg antiferromagnetic chain. Disorder is inversely related to the gap G of the initial rectangular distribution and $G_c \approx 0.45$ [44].

the system flows to an *infinite randomness fixed point* or random singlet phase [44]. This becomes clear when we obtain the fixed point form of the probability distribution of interactions for $G = 0$, which turns out to be given by Eq. 6. The exponent α as a function of the cut-off Ω is shown in Fig. 16 and varies as in Eq. 7. This behavior characterizes the strong disorder case, $G = 0$, as a random singlet phase [47].

Further evidence for a random singlet phase at $G = 0$ is obtained considering the fraction of remaining active spins ρ as a function of the energy scale set by the cut-off Ω [47]. In Fig. 17 the density $\rho = 1/L$ is shown as a function of the cut-off [44]. From this expression the exponent ψ appearing in Eq. 8 is extracted. As expected it takes the value $\psi = 1/2$ characteristic of the random singlet phase [47].

Finally, the distribution of first gaps [55, 56, 57, 58] at $G = 0$ is calculated. This is obtained starting from a given configuration of random interactions for a chain of size L and eliminating the spins, as described above, until a single pair remains. The interaction between these remaining spins yields the first gap Δ for excitation. Implementing this procedure for a large number of initial random configurations for chains of different sizes

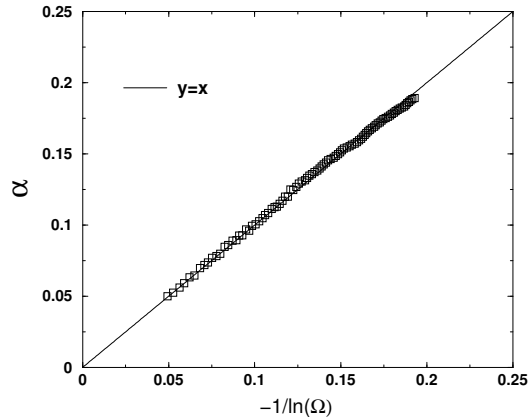


Figure 16: Exponent α of the fixed point, power law distribution, Eq. 7, as a function of the cut-off Ω in the low energy limit [44].

L yields the distributions $P_L(\log \Delta)$ shown in Fig. 18. We considered over 10^4 initial configurations to obtain the gap distributions. The widths of these distributions increase without limit as the sizes L of the chains increase, as expected for an infinite randomness fixed point.

According to the scaling form relating energy and length, Eq. 8, it is expected that the distribution $P(-\log \Delta/L^\psi)$ will present a universal behavior, independent of the size L of the chains when plotted versus the variable $-\log \Delta/L^\psi$. This is indeed the case for $G = 0$ as shown in Fig. 18 for the random singlet phase exponent $\psi = 1/2$.

We now decrease disorder increasing the gap in the exchange distribution. Figure 19 shows the first gap distributions for different degrees of disorder as characterized by the gaps G in the initial distribution of interactions. In all cases investigated with $G \neq 0$, it is found that the first gap distributions saturate at low energies in a form described by the expression, $P(\log \Delta) \sim \Delta^{1/Z}$ for $\Delta \rightarrow 0$. The *dynamic exponent* Z becomes independent of L for L sufficiently large. Large chains have to be considered in order to observe this effect. We find $Z_\infty \sim 10.87$, $Z_\infty \sim 1.01$ and $Z_\infty \sim 0.68$ for $G = 0.1$, $G = 0.45$ and $G = 0.5$, respectively. From these values of the dynamic exponent it is possible to deduce the existence of a Griffiths phase extending up to $G_G \approx 0.45$ where the dynamic exponent reaches the value $Z = 1$ [44] (see Fig. 15). For values of the gap $G > G_G$, i.e., small disorder, the dynamic exponent $Z < 1$. The distribution of first gap for excitations, from which low temperature thermodynamic properties can be deduced, implies that $Z > 1$ is required to obtain a singular behavior for these quantities with decreasing temperature. Consequently at G_G there is a significant change in the nature of the thermodynamic behavior of the system. The phase for $G > G_G$ is a disordered Haldane phase with a pseudo-gap in the excitation spectrum (see Fig. 15).

We now consider spin-3/2 chains [59]. For these chains, after elimination of the strongest coupled pair, the MDH method yields for the new coupling between their neighbors,

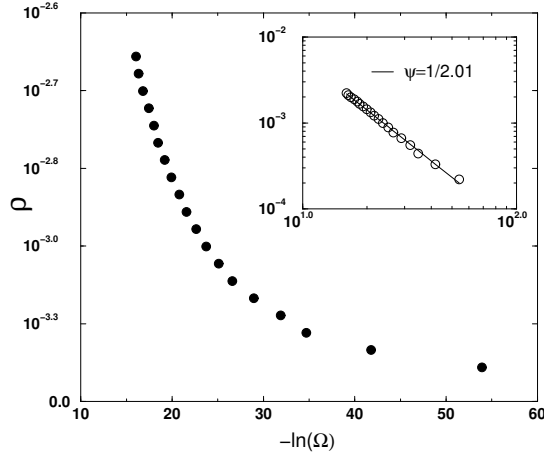


Figure 17: The density of active spins as a function of the cut-off in the low energy limit. The inset shows the expected behavior for a random singlet phase with the exponent $\psi \approx 1/2$ [44].

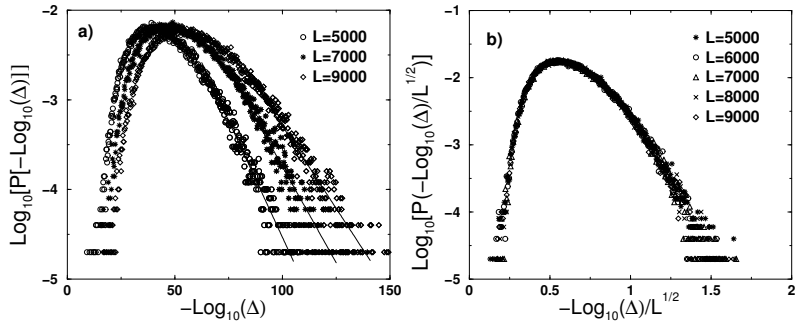


Figure 18: a) Probability distribution of the first gap at the transition point, $G = 0$. The distribution become broader and broader with L , which signals infinite randomness behavior. b) Scaling plot for the gap distributions. The collapse of the curves is obtained for $\psi = 1/2$ as expected for a random singlet phase [44].

$$J' = \frac{5 J_1 J_2}{2 \Omega} \quad (14)$$

Consider the case $J_1 \geq J_2$. For $J_1 > (2/5)\Omega$ the new effective interaction J' is necessarily larger than one of those eliminated, in this case, than J_2 . In order to deal with this problem, the MDH method has again to be generalized. If the largest neighboring interaction to Ω , $J_1 < (2/5)\Omega$, then we eliminate the strongest coupled pair obtaining an effective interaction between the neighbors to this pair which is given by Eq. 14 (see Fig. 13a). This new effective interaction is always smaller than those eliminated. Now suppose $J_1 > J_2$ and $J_1 > (2/5)\Omega$. In this case, we consider the *trio* of spins $S = 3/2$ coupled by the two strongest interactions of the trio, J_1 and Ω and solve it exactly (see Fig. 13b). The ground state of this trio of spins $S = 3/2$ is a degenerate quadruplet. It will be substituted by an effective spin- $3/2$ interacting with its neighbors through *new renormalized* interactions

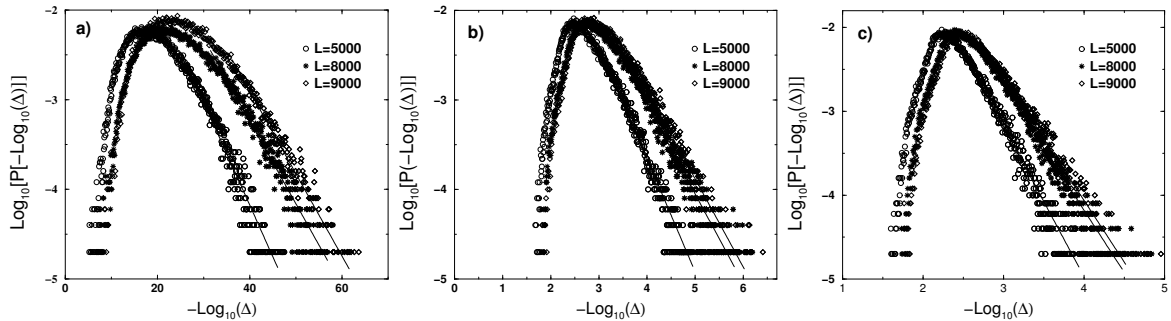


Figure 19: Probability distributions of the first gap obtained from initial rectangular distributions of couplings with a gap G and different systems sizes L [44]. For clarity not all values of L are shown. The solid lines represent best fits to the form $\log_{10}[P(-\log_{10} \Delta)] = A_L - \frac{1}{Z_L} \log_{10} \Delta$. a) $G = 0.1$, $Z_{5000} = 8.69$, $Z_{6000} = 8.70$, $Z_{7000} = 10.45$, $Z_{8000} = 10.85$ and $Z_{9000} = 10.87$. b) $G = 0.45$, $Z_{5000} = 0.79$, $Z_{6000} = 0.81$, $Z_{7000} = 0.96$, $Z_{8000} = 1.0$ and $Z_{9000} = 1.01$. c) $G = 0.5$, $Z_{5000} = 0.55$, $Z_{6000} = 0.58$, $Z_{7000} = 0.63$, $Z_{8000} = 0.67$ and $Z_{9000} = 0.68$.

obtained by degenerate perturbation theory acting on the ground state of the trio. The 64×64 matrix associated with the trio is diagonalized *analytically*. This allows to obtain results on large chains and to deal with a large numbers of initial configurations. Fig. 20 shows that perturbation theory is now always satisfied. We have considered initial rectangular distributions of interactions with a gap G (see Fig. 11). Even for weak disorder, with a gap as large as $G = 0.5$ in the starting distribution, the method works very well and never an interaction larger than those eliminated is generated.

Figure 21 shows the first gap distributions for different degrees of disorder as characterized by different gaps G in the initial distribution of interactions. For all cases these distributions saturate at low energies in a form described by the expression, $P(-\log \Delta) \sim \Delta^{1/Z}$ for $\Delta \rightarrow 0$. The *dynamic exponent* Z becomes independent of L for L sufficiently large. Again, large chains have to be considered to observe this effect. The phase diagram is such that, for strong disorder which corresponds to $G = 0$, there is a Griffiths phase with a dynamic exponent $Z \sim 12.7$ (see Fig. 21). This phase is characterized by *first gap distributions* [44] that saturate at low energies in the form, $P(-\log \Delta) \sim \Delta^{1/Z}$ for $\Delta \rightarrow 0$. We find $Z_\infty \sim 0.43$ and $Z_\infty \sim 1.12$ for $G = 0.2$ and $G = 0.12$, respectively, from which the existence of a Griffiths phase extending up to $G_c \approx 0.11$ is deduced. At this point the dynamic exponent reaches the value $Z = 1$. Since, for example, the susceptibility $\chi \propto T^{1-Z}$, a singular low temperature behavior implies $Z > 1$. At G_c there is in fact a significant change in the nature of the thermodynamic behavior of the system [60]. The phase for $G > G_c$ is one with quasi-long range order, i.e., with spin correlations decaying algebraically with distance, similar to the zero temperature phase of the pure chain [60].

In order to check the possibility of a random singlet phase in the spin- $3/2$ chain we consider another class of distributions of exchange couplings associated with *extreme* disorder. These distributions are of the form, $P(J) \propto J^{-1+1/\gamma}$. For $\gamma = 1$ this reduces to the gapless case of rectangular distributions considered previously and for $\gamma > 1$, we

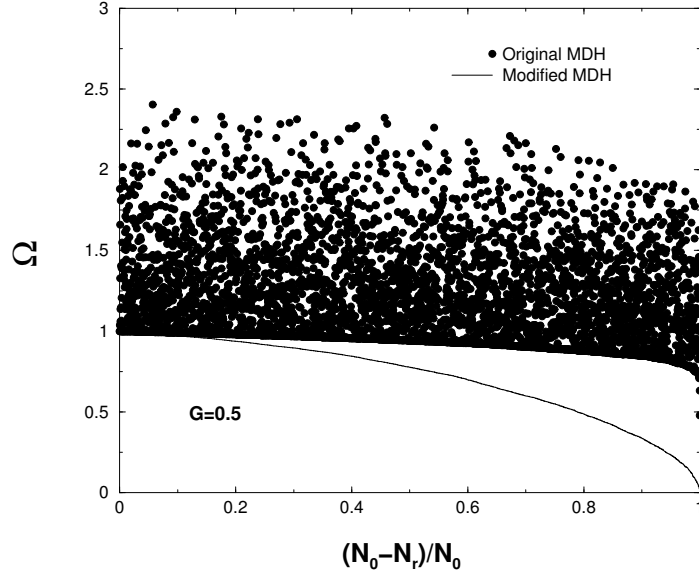


Figure 20: The evolution of the cut-off, for an initial rectangular distribution with $G = 0.5$, along the renormalization process of the spin-3/2 REHAC. The results for the original MDH and the present (modified) renormalization group procedures are shown [59].

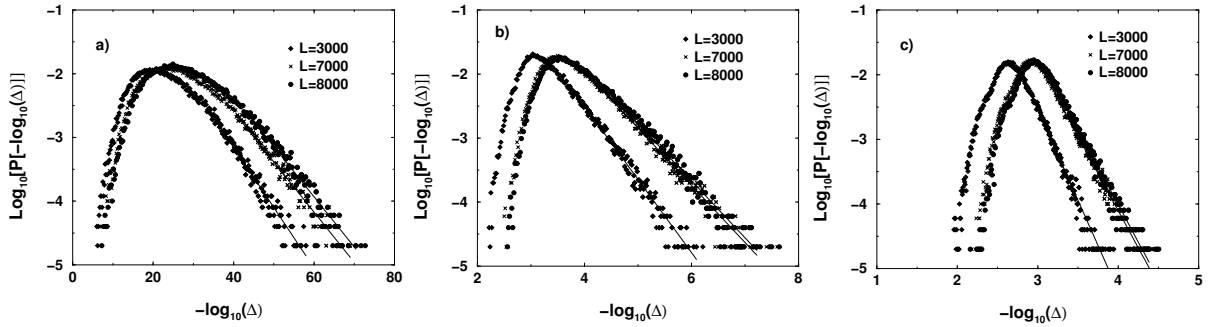


Figure 21: Probability distributions of *first gap* for initial rectangular distributions of couplings with gaps G and different systems sizes L [59]. For clarity not all values of L are shown. The solid lines represent best fits to the form $\log_{10}[P(-\log_{10} \Delta)] = A_L - \frac{1}{Z_L} \log_{10} \Delta$. a) $G = 0$, $Z_{3000} = 10.51$, $Z_{7000} = 12.68$, and $Z_{8000} = 12.70$. b) $G = 0.12$, $Z_{3000} = 0.87$, $Z_{7000} = 1.11$, and $Z_{8000} = 1.12$. c) $G = 0.2$, $Z_{3000} = 0.35$, $Z_{7000} = 0.43$, and $Z_{8000} = 0.43$.

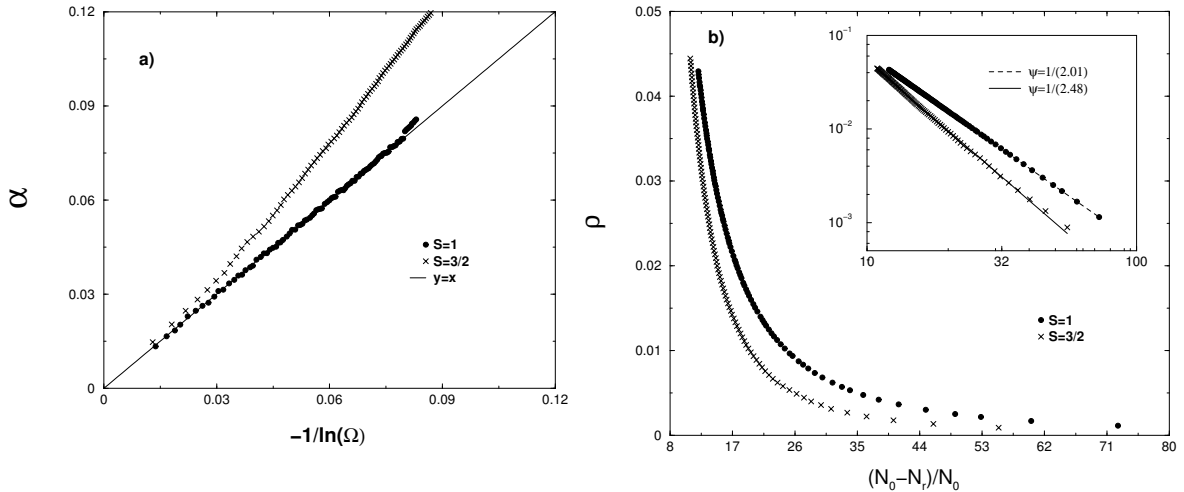


Figure 22: a) The exponent α describing the asymptotic low energy behavior of the renormalized exchange distribution as a function of the scale dependent cut-off. b) Fraction of active spins as a function of the cut-off [59]. For comparison the results for the spin-1 and spin-3/2 REHACs are shown. In both cases the starting distribution is extremely disordered with $\gamma = 20$ (see text).

have the extreme disordered cases. We now report our results for the random spin-3/2 chain obtained with the modified renormalization group procedure [44] for the case of an extremely disordered distribution with $\gamma = 20$ [59]. In the random singlet phase the fixed point distribution of interactions attained when the cut-off Ω is sufficiently reduced takes the form given by Eq. 6. Fig. 22a shows the exponents α of this equation obtained from the asymptotic form of the exchange distributions after the cut-off Ω has been sufficiently reduced. For comparison, the results for a spin-1 REHAC with the same original extreme disorder distribution are shown. In this case a random singlet phase is clearly established. Chains of size as large as $L = 4.5 \times 10^5$ have been considered in these calculations. Fig. 22b shows the density $\rho = 1/L$ of active spins as a function of the cut-off Ω (see Eq. 8). From this expression the exponent ψ (see Eq. 8) has been extracted. It takes the value $\psi = 1/(2.4)$ which is close to the value $\psi = 1/2$ expected for a random singlet phase [47]. As shown in this figure, for comparison, the spin-1 chain has clearly converged to this phase within the same scale of the cut-offs. These results suggest that in this case of extreme disorder, the spin-3/2 REHAC eventually reaches a random singlet phase, although the convergence is very slow.

The MDH elimination procedure can be generalized for finite temperatures and arbitrary spins S . It is given by [59]

$$J' = \frac{2}{3}S(S+1)\frac{J_1J_2}{\Omega}W_S(\beta\Omega) \quad (15)$$

where

$$W_S(y) = \frac{(2S+1)^2 - \sum_{i=0}^{2S} (2i+1)e^{-\frac{1}{2}i(i+1)y} \left[1 + \frac{1}{2}i(i+1)\right]}{4S(S+1) \sum_{i=0}^{2S} (2i+1)e^{-\frac{1}{2}i(i+1)y}} \quad (16)$$

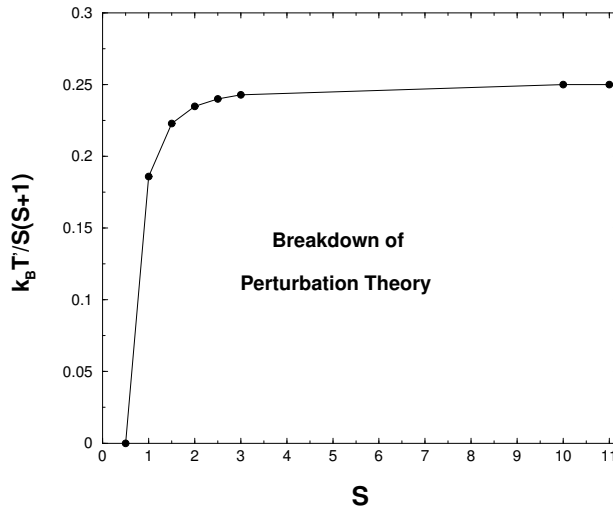


Figure 23: Temperature T^* below which the MDH perturbation theory breaks down for different values of the spin S . The energy $k_B T^*$ is in units of the cut-off Ω of the original exchange distribution [59].

Notice that for sufficiently high temperatures, the factor $\frac{2}{3}S(S+1)W_S(\beta\Omega) < 1$ and the MDH elimination procedure works in this case [49, 61, 62, 63, 64]. A random singlet phase is reached in the sense that the asymptotic distribution of exchange attains the form given by Eq. 6 at these temperatures. However, as T is reduced the problem becomes essentially non-perturbative for spins $S \geq 1$, as the equation above generates coupling larger than those eliminated. In particular at $T = 0$ the excited states which reduce the factor W_S from its value $W_S(T = 0) = 1$ are now frozen. In fact *none* of the excited states play a role in the problem at zero temperature. Notice that in the generalized renormalization scheme, degenerate perturbation theory is applied to the *ground state* of the spin trio. This is possibly the main reason for the discrepancy between the results above and those obtained by the authors of Refs. [61, 64]. These authors find that quantum chains of arbitrary spin- S present random singlet phases even for weak disorder. The consideration of excited states in the problem favors the appearance of an infinite disorder random singlet phase, as occurs at finite temperatures.

In the limit $S \rightarrow \infty$ and $T \rightarrow 0$, replacing the sum by an integral and with a proper renormalization of the Hamiltonian, Eqs. 15 and 16 yield $J' = J_1 J_2 / 4k_B T$, in agreement with the result of Ref. [46] for classical spins. In Fig. 23 it is shown the temperature T^* below which the simple perturbative approach breaks down, for a given value of the spin of the random chain.

Notice that for rectangular distributions, the Griffiths phase of the spin-1 REHAC extends up to $G_c = 0.45$ and for spin-3/2 up to $G_c = 0.11$. For random classical spin chains, the susceptibility $\chi \propto P(0)|\ln T|$ where $P(0)$ is the finite weight at the origin of the original distribution $P(J)$ [46]. This weak logarithmic singularity is similar to that expected for quantum chains at the border of the Griffiths phase ($Z \approx 1$) as if in this case

of classical spins and rectangular distribution, $G_c = 0$.

Then for rectangular distributions, the spin-3/2 REHAC presents a Griffiths phase up to a critical value of disorder. For extreme disorder, where the starting exchange distributions are singular for small values of the coupling our results only suggest that a random singlet phase will be asymptotically reached as the cut-off of the distribution $\Omega \rightarrow 0$. These results are consistent with those of Refs. [60] that find a random singlet phase in spin-3/2 chains for the case of extremely disordered distributions.

It is clear by now that the power law temperature dependent behavior observed in the magnetic susceptibility and other thermodynamic properties of the low dimensional oxy-borates can be traced to the mapping of their low dimensional magnetic structures to a random chain problem. The details of this mapping have yet to be explored. The oxy-borates were the first class of inorganic materials where this kind of low dimensional magnetic behavior has been found. They provide a strong motivation to make further theoretical progress in this problem and of other quantum systems with disorder [65].

We would like to thank Conselho Nacional de Desenvolvimento Científico e Tecnológico-CNPq-Brasil and Fundação de Amparo a Pesquisa do Estado do Rio de Janeiro-FAPERJ (PRONEX/CNPq-FAPERJ-E-26/171.168/2003) for partial financial support.

References

- [1] C. Klein in, *Manual of Mineral Science, 22nd edition*: after James D. Dana; with continued contribution of Cornelius S. Hurlbut, Jr. Publisher: J.Wiley, New York, (2002).
- [2] R. Norrestam, *Z. fur Kristall.* **189** (1989) 1.
- [3] R. Norrestam, M. Kritikos, and A. Sjodin, *J. Sol. State Chemistry.* **114** (1995) 311.
- [4] J.P. Attfield, A.M.T. Bell, L.M. Rodriguez-Martinez, J.M. Greneche, R.J. Cernik, J.F. Clarke, and D.A. Perkins, *Nature* **396** (1998) 655.
- [5] J.P. Attfield, A.M.T. Bell, L.M. Rodriguez-Martinez, J.M. Greneche, R. Retoux, M. Leblanc, R.J. Cernik, J.F. Clarke, and D.A. Perkins, *J. Mater. Chem.* **9** (1999) 205; A. D. Balaev, O. A. Bayukov, A. D. Vasil'ev, D. A. Velikanov, N. B. Ivanova, N. V. Kazak, S. G. Ovchinnikov, M. Abd-Elmeguid, and V. V. Rudenko, *JETP* **97** (2003) 989.
- [6] J.J. Capponi, J. Chenevas, and J.C. Joubert, *J. Solid State Phys.* **7** (1973) 49.
- [7] R.B. Guimarães, J.C. Fernandes, M.A. Continentino, H.A. Borges, C.S. Moura, J.B.M. da Cunha, and C.A. dos Santos, *Phys. Rev B* **56** (1997) 292.
- [8] R. Norrestam, K. Nielsen, I. Sotofte, and N. Thorup, *Zeit. fur Kristall.* **189** (1989) 33.
- [9] M.A. Continentino, J.C. Fernandes, R.B. Guimarães, H.A. Borges, A. Sulpice, J-L. Tholence, J.L. Siqueira, J.B.M. Cunha, and C.A. dos Santos, *Eur. Phys. J.* **9** (1999) 613.
- [10] D.A. Konnert, D.E. Applemen, J.R. Clark, W.L. Finger, T. Kato, and Y. Miura, *Am. Mineral.* **61** (1976) 116.
- [11] P.B. Moore and T. Araki, *Am. Mineral.* **59** (1974) 985.
- [12] Y. Takeuchi, N. Haga, T. Kato, and Y. Miura, *Can. Mineral.* **16** (1978) 475.
- [13] J.-O. Bovin and M. O'Keeffe, *Acta Cryst.* **A37** (1981) 35.
- [14] J.-O. Bovin, A. Carlsson, R. Sjovall, R. Thomasson, R. Norrestam, and I. Sotofte, *Z. fur Kristall.* **211** (1996) 440.
- [15] R. Norrestam and J.-O. Bovin, *Zeit. fur Kristall.* **181** (1987) 135.
- [16] M. Mir, R.B. Guimarães, J.C. Fernandes, M.A. Continentino, A.C. Doriguetto, Y.P. Mascarenhas, J. Ellena, E.E. Castellano, R.S. Freitas, and L. Ghivelder, *Phys. Rev. Lett.* **87** (2001) 147201.

- [17] J.C. Fernandes, F.S. Sarrat, R.B. Guimarães, R.S. Freitas, M.A. Continentino, A.C. Doriguetto, Y.P. Mascarenhas, J. Ellena, E.E. Castellano, J-L. Tholence, J. Dumas, and L. Ghivelder, *Phys. Rev. B* **67** (2003) 104413.
- [18] A. Utzolino and K. Bluhm, *Zeit. Naturforsch.* **51b** (1996) 912.
- [19] J.C. Fernandes, R.B. Guimarães, M.A. Continentino, R. Rapp, J-L. Tholence, J. Dumas, Y. Blancquaert, S. Yates, and C. Paulsen, *Phys. Rev B* **69** (2004) 054418.
- [20] A. Wiedenmann and P. Burlet, *J. Physique* **39** supplement au *n*°8 (1978) C6-720.
- [21] A. Wiedenmann, P. Burlet, and R. Chevalier, *J. Mag. Mag. Matt.* **15-18** (1980) 216.
- [22] J.C. Fernandes, R.B. Guimarães, M.A. Continentino, H.A. Borges, J.V. Valarelli, and Alex Lacerda, *Phys. Rev. B* **50** (1994) 16754.
- [23] L.N. Boulaevskii, A.V. Zvarykina, Yu. S. Karimov, R.B. Lyubovskii, and I.F. Shchegolev, *Sov. Phys. JETP* **35** (1972) 384.
- [24] M. Matos, R. Hoffmann, A. Latgé, and E. V. Anda, *Chem. Mater.* **8** (1996) 2324.
- [25] D. C. Marcucci, A. Latgé, E. V. Anda, M. Matos, and J.C. Fernandes, *Phys. Rev. B* **56** (1997) 3672.
- [26] M.A. Continentino, A.M. Pedreira, R.B. Guimarães, M.Mir, J.C. Fernandes, R.S. Freitas, and L. Ghivelder, *Phys. Rev B* **64** (2001) 014406.
- [27] M.A. Continentino, J.C. Fernandes, R.B. Guimarães, B. Boechat, H.A. Borges, J.V. Valarelli, E. Haanappel, A. Lacerda, and P.R.J. Silva, *Philos. Mag. B* **73** (1996) 601.
- [28] M. Brunner, J.-L. Tholence, L. Puech, S. Haan, J.J. Capponi, R. Calemczuk, J.C. Fernandes, and M.A. Continentino, *Physica B* **233** (1997) 37.
- [29] J.C. Fernandes, R.B. Guimarães, M.A. Continentino, H.A. Borges, A. Sulpice, J.-L. Tholence, J.L. Siqueira, L.I. Zawislak, J.B.M. da Cunha, and C.A. dos Santos, *Phys. Rev. B* **58** (1998) 287.
- [30] M.A. Continentino, J.C. Fernandes, R.B. Guimarães, H.A. Borges, A. Sulpice, J.-L. Tholence, J.L. Siqueira, J.B.M. da Cunha, and C.A. dos Santos, *Eur. Phys. J.* **9** (1999) 613.
- [31] R.B. Guimarães, M. Mir, J.C. Fernandes, M.A. Continentino, H.A. Borges, G. Cernicchiaro, M.B. Fontes, D.R.S. Candela, and E.M. Baggio-Saitovitch, *Phys. Rev. B* **60** (1999) 6617.
- [32] H. Neuendorf and W. Gunsser, *J. Mag. Mag. Matt.* **173** (1997) 117.
- [33] A. P. Douvalis, V. Papaefthymiou, A. Moukarika, and T. Bakas, *Hyperf. Interactions* **126** (2000) 319.

- [34] R.J. Goff, A.J. Williams, and J.P. Attfield, Phys. Rev. B **70** (2004) 014426.
- [35] J.P. Attfield, J.F. Clarke, and D.A. Perkins, Physica B **180 & 181** (1992) 581.
- [36] J.C. Fernandes, R.B. Guimarães, M.A. Continentino, L. Ghivelder, and R.S. Freitas, Phys. Rev. B **61** (2000) R850.
- [37] J.S. Swinea and H. Steinfink, Am. Mineral. **68** (1983) 827.
- [38] J. Larrea, D.R. Sanchez, F.J. Litterst, and E.M. Baggio-Saitovitch, J. Phys.: Condens. Matter **13** (2001) L949.
- [39] A. Latgé and M.A. Continentino, Phys. Rev. B **66** (2002) 094113.
- [40] M. Whangbo, H.-J. Koo, J. Dumas, and M.A. Continentino, Inorg. Chem. **41** (2002) 2193.
- [41] for a review see E. Dagotto and T. M. Rice, Science **271** (1996) 618.
- [42] J. A. Hoyos and E. Miranda, Phys. Rev. **B 69** (2004) 214411.
- [43] R. Mélin, Y.-C. Lin, P. Lajkó, H. Rieger, and F. Iglói, Phys. Rev. **B 65** (2002) 104415; E. Yusuf and K. Yang, Phys. Rev. **B 65** (2002) 224428; E. Yusuf and K. Yang, Phys. Rev. **B 68** (2003) 024425.
- [44] A. Saguia, B. Boechat, and M. A. Continentino, Phys. Rev. Lett **89** (2002) 117202.
- [45] E. Westerberger, A. Furusaki, M. Sigrist, and P. A. Lee, Phys. Rev. **B 55** (1997) 12578; T. Hikihara, A. Furusaki, and M. Sigrist, Phys. Rev. **B 60** (1999) 12116.
- [46] S.K. Ma, C. Dasgupta, and C.K. Hu, Phys. Rev. Lett. **43** (1979) 1434; S.K. Ma and C. Dasgupta, Phys. Rev. **B 22** (1980) 1305.
- [47] D.S. Fisher, Phys. Rev. **B 50** (1994) 3799; Phys. Rev. **B 51** (1995) 6411.
- [48] B. Boechat, A. Saguia, and M.A. Continentino, Solid State. Commun. **98** (1996) 411.
- [49] R.A. Hyman and K. Yang, Phys. Rev. Lett. **78** (1997) 1783.
- [50] K. Hida, Phys. Rev. **B 45** (1992) 2207.
- [51] K. Hida, Phys. Rev. Lett. **83** (1999) 3297.
- [52] S. Bergkvist, P. Henelius, and A. Rosengren, Phys. Rev. **B 66** (2002) 134407; S. Todo, K. Kato, and H. Takayama, J. Phys. Soc. Jpn. **69** (2000) A355.
- [53] A. Saguia, B. Boechat, and M.A. Continentino, Phys. Rev. **B 58** (1998) 58; Phys. Rev. **B 62** (2000) 5541.
- [54] A. Saguia, B. Boechat, and M.A. Continentino, Phys. Rev. **B 63** (2001) 52414.

- [55] R. Mélin, Y.-C. Lin, P. Lajkó, H. Rieger, and F. Iglói, Phys. Rev. **B 65** (2002) 104415.
- [56] Y.-C. Lin, N. Kawashima, F. Iglói, and H. Rieger, Prog. Theor. Phys. Suppl. **138** (2000) 470.
- [57] F. Iglói, Phys. Rev. **B 65** (2002) 064416.
- [58] E. Carlon, P. Lajkó, and F. Iglói, Phys. Rev. Lett. **87** (2001) 277201.
- [59] A. Saguia, B. Boechat, and M. A. Continentino Phys. Rev. **B 68** (2003) 020403(R).
- [60] E. Carlon, P. Lajk, H. Rieger, and F. Iglí, Phys. Rev. **B 69** (2004) 144416.
- [61] G. Refael, S. Kehrein, and D.S. Fisher, Phys. Rev. **B 66** (2002) R060402.
- [62] K. Damle, Phys. Rev. **B 66** (2002) 104425.
- [63] C. Monthus, O. Golinelli, and Th. Jolicoeur, Phys. Rev. Lett. **79** (1997) 3254; Phys. Rev. **B 58** (1998) 805.
- [64] K. Damle and D. A. Huse, Phys. Rev. Lett. **89** (2002) 277203.
- [65] see *Quantum Scaling in Many-body Systems*, M. A. Continentino (World Scientific, Singapore) 2001.